

Figure 1.1. Classical interpretation of ESR spectroscopy. (a) Free precession of the magnetization M of an ensemble of isolated electrons around the static magnetic field B_0 with Larmor angular frequency $\omega_0 = \gamma B_0$, γ being the magnetogyric ratio. The transverse magnetization oscillates at the same frequency. (b) In condensed matter, the electrons exchange energy with the surroundings. A rotating microwave field $B_1(t) \perp B_0$ with angular frequency ω forces the precession of the magnetization around B_0 with the same angular frequency. When $\omega \simeq \omega_0$, an absorption resonance occurs. Adapted from Ref. [26].

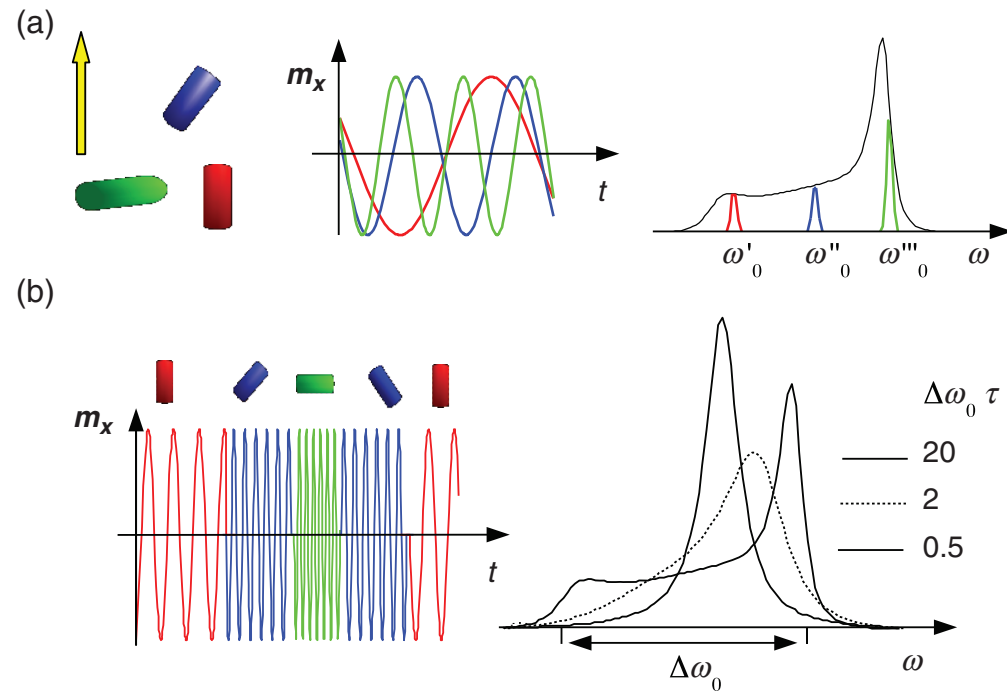


Figure 1.3. ESR lineshapes of spin probes in frozen (a) and mobile (b) hosts. **(a)** The magnetic dipoles m of immobile spin probes in a frozen liquid have different ω_0 values due to their different orientations with respect to B_0 , thus resulting in a broad line with width $\Delta\omega_0$ (black line), usually referred to as rigid-limit or powder lineshape. **(b)** If the spin probe undergoes rotation (sketched as instantaneous clockwise jumps at random times), ω_0 fluctuates. When the rotational rate $1/\tau$ is larger than the width of the ω_0 distribution $\Delta\omega_0$, the different precession frequencies become indistinguishable and an average value is seen, that is, the ESR lineshape coalesces (motional narrowing) [4,14]. Adapted from Ref. [26].

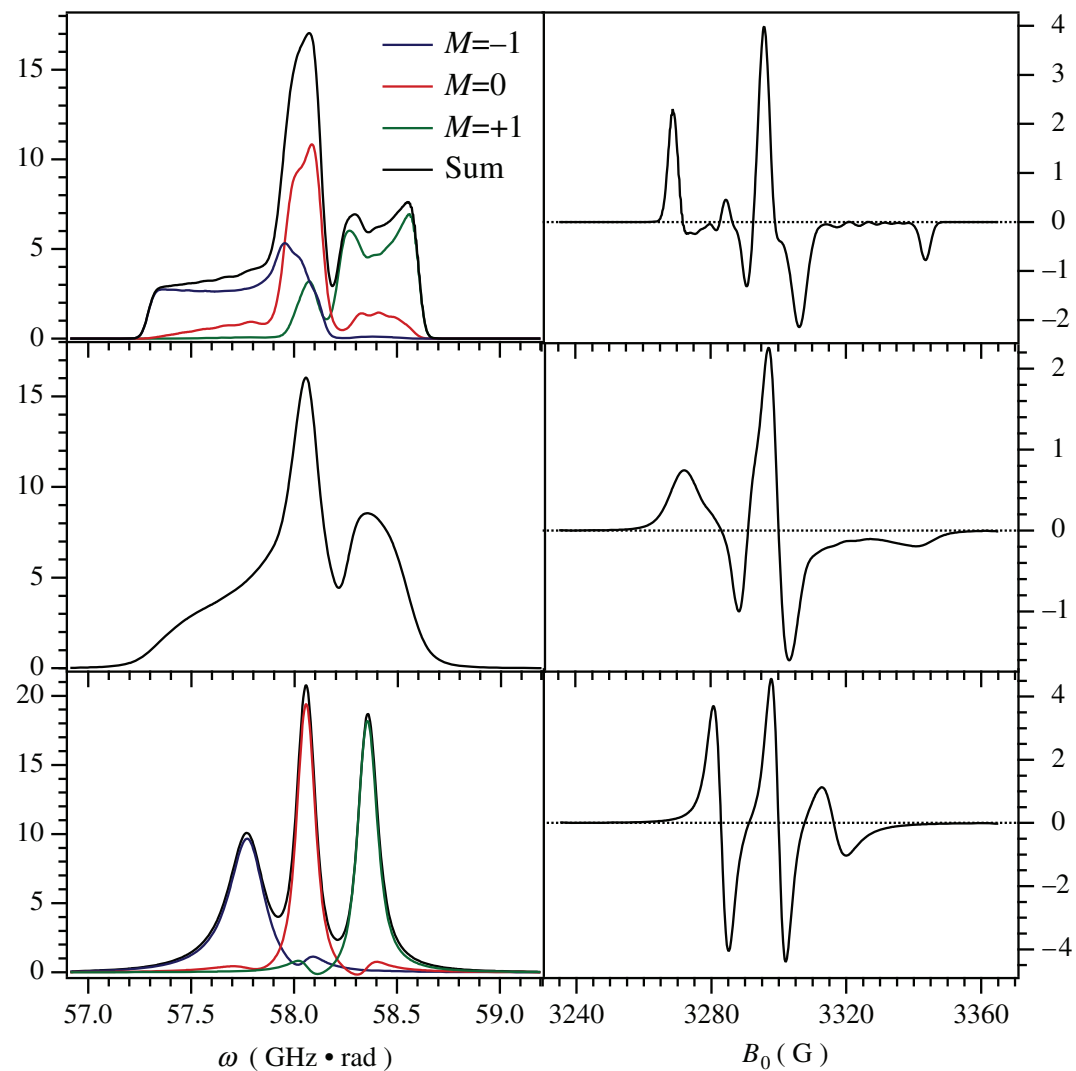


Figure 1.6. ESR lineshapes of a nitroxide spin probe (g tensor as in Fig. 5, $A_x = 18.76$ MHz, $A_y = 19.88$ MHz, $A_z = 104.4$ MHz, $T_2^* = 56$ ns) undergoing reorientation with jump angle $\theta = 80^\circ$ and rotational correlation times $\tau = 860$ (top), 9.04 (middle), 1.81 ns (bottom). Left: Absorption versus frequency of the microwave field for constant magnetic field $B_0^* = 3300$ G. Right: Absorption in derivative mode versus static magnetic field for constant microwave frequency $\omega^* = 58.05$ rad · GHz. The lineshapes with $\tau = 860$ ns (top panel) are virtually coincident with the powder lineshapes corresponding to immobile spin probes in a frozen host. In that case the three hyperfine components with $M = \pm 1, 0$, corresponding to the three possible transitions (see Fig. 2, bottom), are explicitly shown. The motional narrowing [4,14,15] reduces the three components to three distinct lines when the spin probe rotates fast (bottom panel).

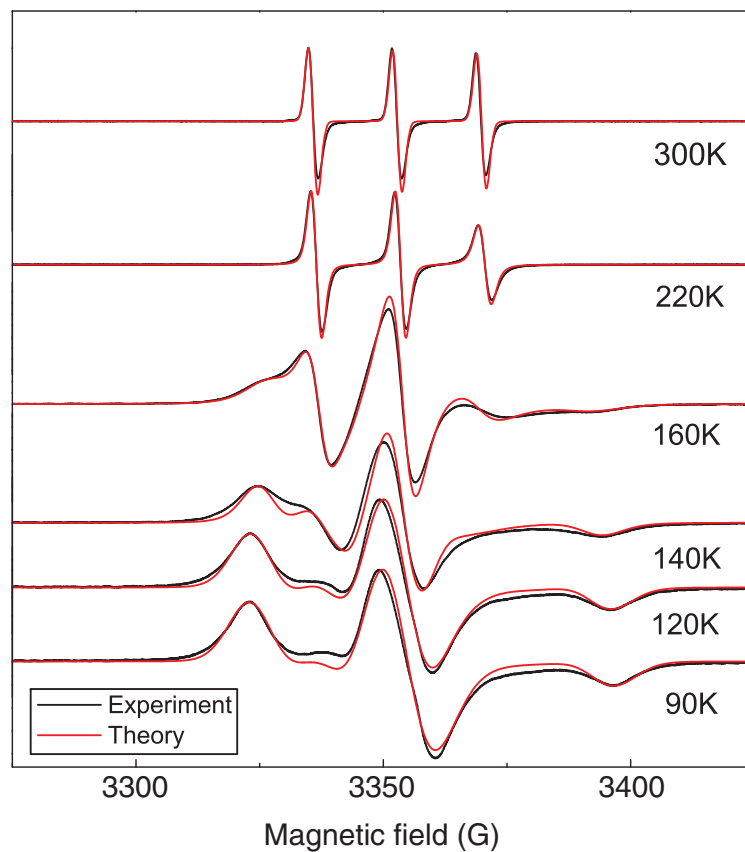


Figure 1.7. Selected ESR lineshapes of the spin probe TEMPOL (see Fig. 2a) in quenched bulk water and subsequent reheating at the indicated temperature. Note that (i) for technical convenience the static magnetic field \mathbf{B}_0 , and not the microwave frequency ω as in Fig. 2b, is swept; (ii) the phase-sensitive detection displays the lineshape in derivative mode. Adapted from Ref. [26].

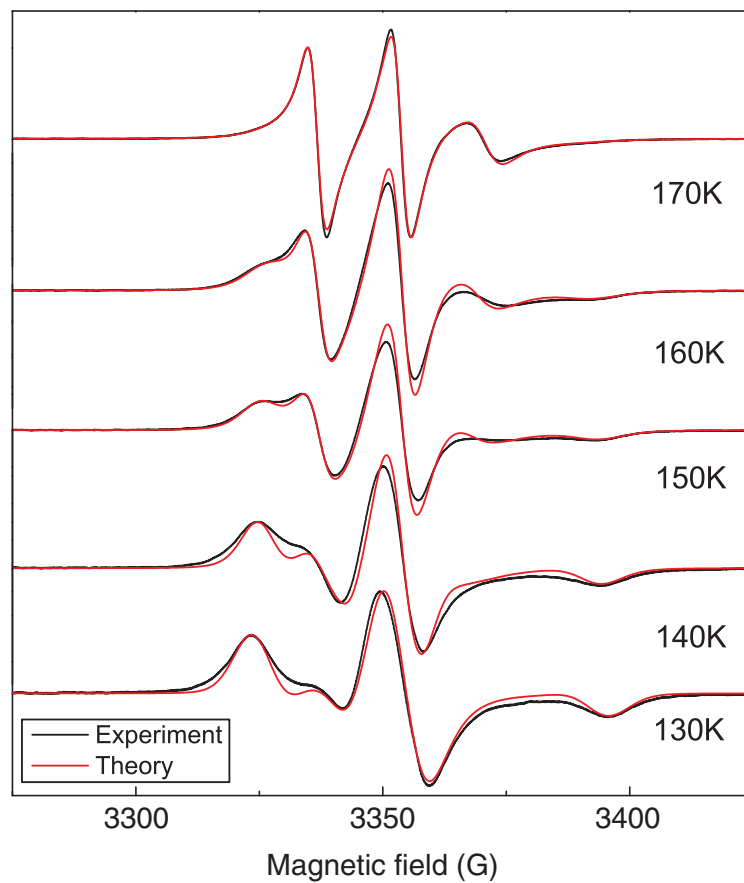


Figure 1.8. ESR lineshapes of TEMPOL in DH regime. Note the growth of the two narrow lines at ~ 3340 and ~ 3360 G that superimpose to the overall lineshape with increasing temperature. Further analysis is presented in Fig. 9. Adapted from Ref. [26].

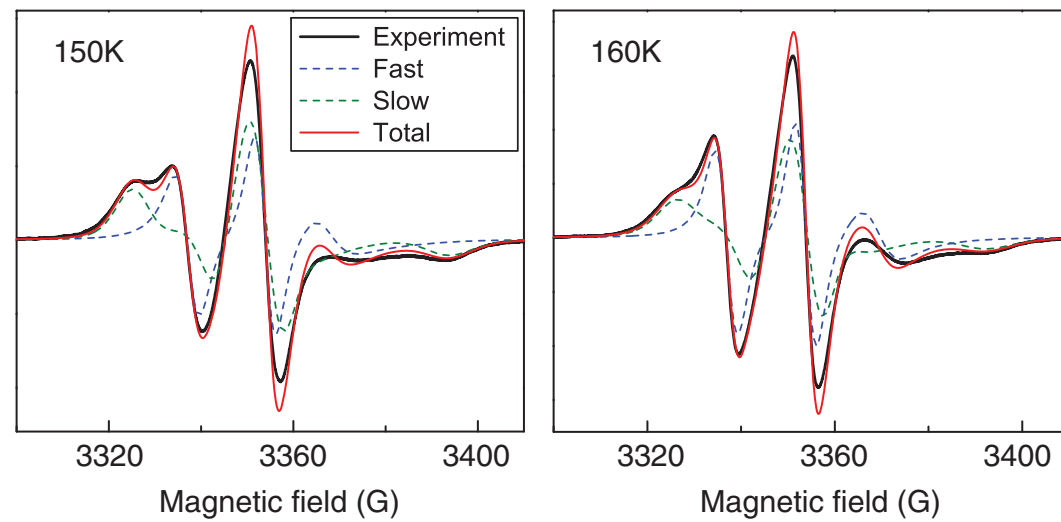


Figure 1.9. Fast (blue) and slow (green) components of the overall lineshape (red) of TEMPOL at two temperatures in DH regime. Adapted from Ref. [26].

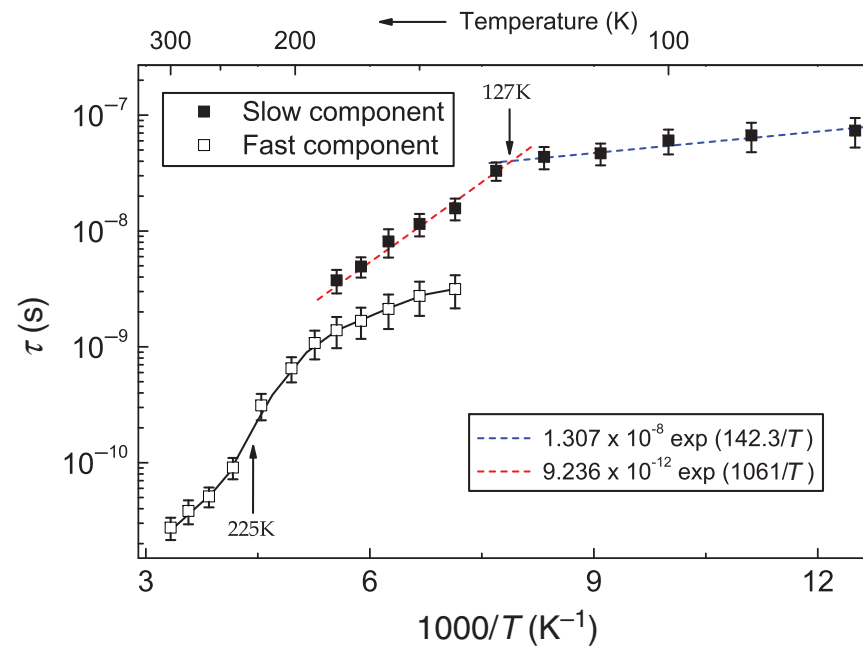


Figure 1.11. Temperature dependence of the rotational correlation times τ_f and τ_s of the fast (F) and the slow (S) fractions of TEMPOL in deeply supercooled bulk water, respectively. Note (i) the knee at $\sim 127\text{K}$ close to $T_g = 136\text{K}$, (ii) the DH regime (140–180K), where the two coexisting TEMPOL fractions with different mobilities are evidenced, (iii) the inflection close to $T_{\text{FSC}} \sim 228\text{K}$. Adapted from Ref. [26].

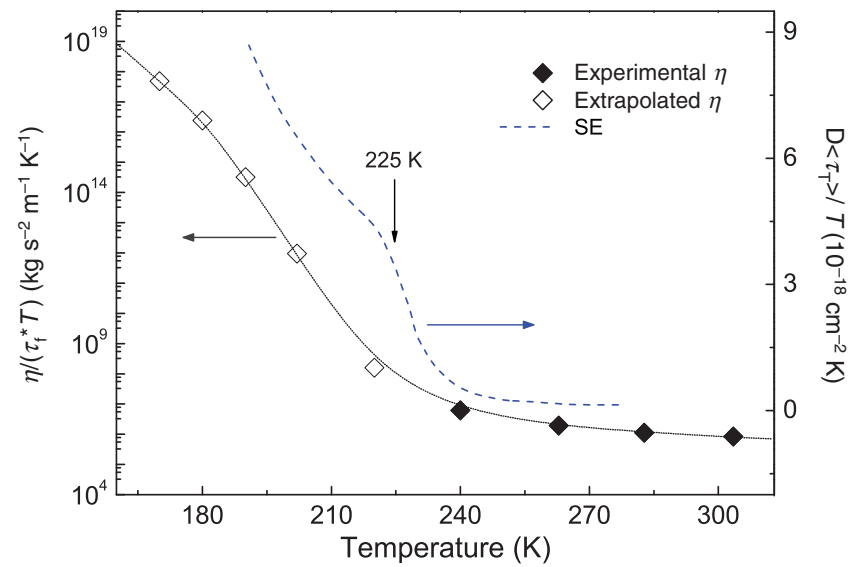


Figure 1.12. Breakdown of the DSE law. Data are compared to the SE breakdown from Ref. [65]. Filled dots refer to temperatures where experimental values of the viscosity are available. Empty dots are based on a thermodynamic extrapolation of the viscosity [69]. The line across the dots is a guide for the eyes. Adapted from Ref. [26].

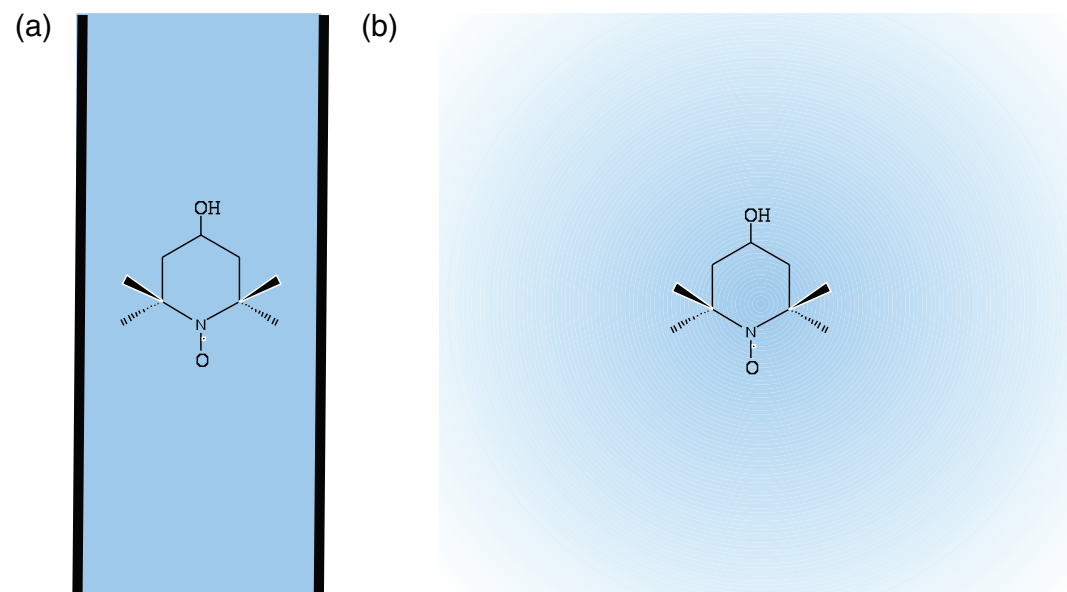


Figure 1.13. Schematic view of TEMPOL in interstitial supercooled (a) and bulk equilibrium (b) “dirty” water. Possible impurities (blue background) expelled by the ice fraction are much more concentrated in supercooled than in equilibrium water.